

# Electronic structure of $\text{SC}_6\text{H}_5$ self-assembled monolayers on $\text{Cu}(111)$ and $\text{Au}(111)$ substrates.

Vasili Perebeinos<sup>1</sup> [\*] and Marshall Newton<sup>2</sup>

<sup>1</sup>Department of Physics,

<sup>2</sup>Department of Chemistry,

Brookhaven National Laboratory,

Upton, New York 1973-5000

(Dated: February 8, 2020)

Recently there has been increased interest in the possibility of using organic molecules as possible electronic components in nanoscale devices. One of the most important issues to be addressed is the role of molecule-surface interactions. We use first principles density functional theory to calculate electronic structure of the phenylthiolate ( $\text{SC}_6\text{H}_5$ ) self-assembled monolayer (SAM) on  $\text{Cu}(111)$  and  $\text{Au}(111)$  substrates. We find lateral dispersion of the molecular states comparable to the charge injection energy at the point, which increases conductance of the SAM compared to the single molecule. We calculate the two photon photoemission spectra (2PPE) and the work function reduction of  $\text{Cu}$  due to the SAM and compare them with the available experimental data. Our results are used to discuss assignments of the observed spectral data and yield predictions for new electronic states due to the monolayer not yet accessed experimentally.

PACS numbers: 71.15.Mb, 73.20.At, 73.40.Ns, 78.68.+m

## I. INTRODUCTION

The purpose of this paper is to elucidate the electronic structure of self-assembled monolayers (SAM) on noble metal substrates. A key quantity which controls the conductance properties of the metal molecule junction is the relative position of the Fermi level on a metal and the molecular states. When a single molecule is attached to a metal substrate, the molecular level becomes a resonance characterized by energy and finite lifetime due to the coupling to the substrate. In the case of a chemisorbed SAM, the molecular orbitals form a two dimensional band structure by two mechanisms: (1) direct exchange between the neighboring orbitals and (2) the substrate mediated interaction. The two mechanisms have different distance dependence, which may be used in optimization of molecular electronic devices.

In the present studies we calculate the band structure of a phenylthiolate (PT) attached to  $\text{Cu}(111)$  and  $\text{Au}(111)$  substrates. We show that the lateral dispersion is significant enough to alter the transport properties of the SAM and has to be taken into account in realistic conductance calculations. We aim to answer three essential questions: (1) to what molecular state the charge injection energy is minimal and therefore the most significant for the conduction properties through the monolayer; (2) how large is the lateral dispersion compared to the charge injection energy at the point; (3) what is the relative contribution of the direct overlap and substrate mediated interaction to the dispersion. In addition we calculate two-photon photoemission (2PPE) spectra and the work function of the SAM/ $\text{Cu}(111)$  system to compare with the experiments by Zhu et. al. [1], which reports two emission peaks, assigned to low lying unoccupied molecular orbitals (LUMO) founded at 3.3 eV and 6.4 eV above the Fermi level. Since the measured work

function was found to be 3.7 eV (compared to 4.9 eV for a clean  $\text{Cu}(111)$  surface), the two LUMO states are, respectively, below and above the vacuum level. We will also refer below to high-lying occupied molecular orbitals (HOMO) and to surface states (SS).

## II. METHOD OF CALCULATION

We use the full potential linearized augmented plane wave (FP-LAPW) method [2] with local orbital extensions [3] in the WIEN2k implementation [4]. The LDA Perdew Wang [5] exchange-correlation potential was used. Well-converged basis sets were employed with a 4.7 Ry plane wave cut off. Five special  $k$ -points were used to sample the two dimensional Brillouin zone. The surface plane was taken as the  $x$ / $y$  plane. We used slab calculations based on a supercell with three metal layers covered on one side by a PT  $\text{SC}_6\text{H}_5$  monolayer for electronic structure calculations, and six metal layers with both sides covered for work function calculations. The PT monolayer is of the so called  $\sqrt{3} \times \sqrt{3}R30^\circ$  type [6], with one molecule per three substrate surface metal atoms. The latter are arranged in a triangular lattice with side  $3R_{\text{M}}$ , where  $R_{\text{M}}$  is the nearest neighbor atom separation. For  $\text{M} = \text{Au}$  and  $\text{Cu}$ , the corresponding cross-section area for molecule is, respectively,  $21.6 \text{ \AA}^2$  and  $16.9 \text{ \AA}^2$  [6, 7]. The cross-sectional mean area of a PT molecule (when directed normal to the substrate) is  $21.1 \text{ \AA}^2$  slightly less than the above value based on the  $\text{Au}$  substrate, thus indicating the possibility of a small degree of tilt [6, 7], whereas no tilt is expected in the case of the  $\text{Cu}$  substrate.

The geometry of the molecular array has been fully relaxed on an unrelaxed substrate with metal atoms in ideal crystal positions. The monolayer on the  $\text{Au}$  substrate

was found tilted by  $18^0$ , consistent with related experimental data [7]. In the calculation, the PT molecule was constrained so as to maintain  $C_{2v}$  intramolecular symmetry. The lowest-energy binding site was Au-Au bridge, analogous to the case of alkanethiols studied by Selloni et. al. [8]. Starting with alignment normal to the substrate, with the projection of the PT plane parallel to a nearest-neighbor Au-Au vector, the PT was tilted in the direction perpendicular to its plane (tilting in the orthogonal direction caused a sharp rise in energy). The calculated tilt relaxation energy per molecule ( $0^0$  to  $18^0$ ) was of the order of  $k_B T$  at room temperature, indicating the likelihood of appreciable thermal fluctuations, similar to the situation noted in [6, 7].

In the case of the Cu substrate we find zero tilt angle for the monolayer due to the close spacing controlled by the Cu lattice constant, with the lowest energy when sulfur binds to the hollow site (where sulfur has four first neighbor Cu atoms). The binding energy for the other hollow site (where S has three first neighbor Cu atoms) is only 10 meV higher in energy, whereas the bridge site is higher by 170 meV.

### III. BAND STRUCTURE RESULTS

When a monolayer of thiolate self assembles on a noble metal substrate, the molecular levels acquire lateral dispersion due to both the direct overlap between the molecules and the substrate-mediated interaction. The direct overlap falls off faster with the distance between the neighboring molecules than the substrate-mediated interactions. In this work we use DFT to study the relative importance of the two contributions and the overall magnitude of the molecular level bandwidths. The electronic structure along the high symmetry direction of the 2-D Brillouin zone is shown in Fig. (1a) for the PT SAM on Cu(111). In order to distinguish which bands originate from the SAM and which are due to the metallic substrate we calculate projected density of states of each band inside the spheres surrounding the atoms of the PT molecule [2, 3]. In addition the band structure of the clean Cu(111) three layer slab is shown in Fig. (1b), at least seven molecular bands due to the SAM can be identified. These molecular bands can be characterized by (1) the energy at the  $\Gamma$ -point, (2) the effective mass for the  $\Gamma$ -M direction in case where a parabolic fit of the dispersion in the vicinity of the  $\Gamma$  point is possible, (3) the bandwidth defined as the energy difference between the M and the  $\Gamma$  point, and (4) the major atomic contributions. These band characteristics are summarized in Table I.

For the copper substrate the molecular levels closest to the Fermi level are the two HOMO's (bands 3 and 4) which are of S (3p) character. They have a very small dispersion (of about 0.2-0.3 eV) and the parabolic fits result in large effective masses ( $\sim 2.0 m_e$ ). The second occupied state (SS<sub>o</sub>, at -0.9 eV) and the second unoccupied

band	E (eV)	$m_{eff}$ ( $m_e$ )	$E_M - E$ (eV)	Character	
	SAM /Cu SAM	SAM /Cu SAM	SAM /Cu SAM		
1	-4.0	-3.6		$C_s$	
2	-2.7	-1.9	-1.5	$C_t$	
3	-1.1	0.30	-2.0	-1.0	S
4	-0.75	0.35	-2.0	-1.2	S
5	1.0	1.6	0.4	0.35	$C_s$
6	2.8	3.7	-0.4	1.0	$C_t$
7	4.0	5.0	-0.3	-0.8	$C_t$
SS <sub>o</sub>	-0.9		0.4		Cu
SS <sub>u</sub>	1.7				Cu
	SAM /Au SAM	SAM /Au SAM	SAM /Au SAM		
1	-2.4	-2.2	0.55	0.8	$C_s$
2	-2.4	-2.1			$C_t$
3	-0.98	0.13	-2.3	-2.7	S
4	-0.85	0.09	1.6	-3.9	S
5	2.75	2.9	1.0	0.95	$C_s$
6	4.1	3.9		0.9	$C_t$
7	4.1	4.3	-0.6	-1.2	$C_t$
SS <sub>o</sub>	-0.45		1.7		Au
SS <sub>u</sub>	1.4		0.5		Au

TABLE I: Analysis of the electronic bandstructure for the PT SAM on Cu(111) SAM on Au(111) and the free molecular arrays at the same geometries. The energies of the bands are given relative to the Fermi level at the  $\Gamma$ -point ( $k = (0;0)$ ). Effective masses are reported for the bands where a parabolic fit (along the  $\Gamma$ -M direction) is possible. The bandwidth is reported for bands where the energy difference between the  $\Gamma$ -point and the M-point can be identified (M denotes  $k = (4 = 3;0)$ ). The last column shows the band character for the SAM/substrate systems, where  $C_s$  stands for side phenyl carbons and  $C_t$  for next to sulfur and top carbons.

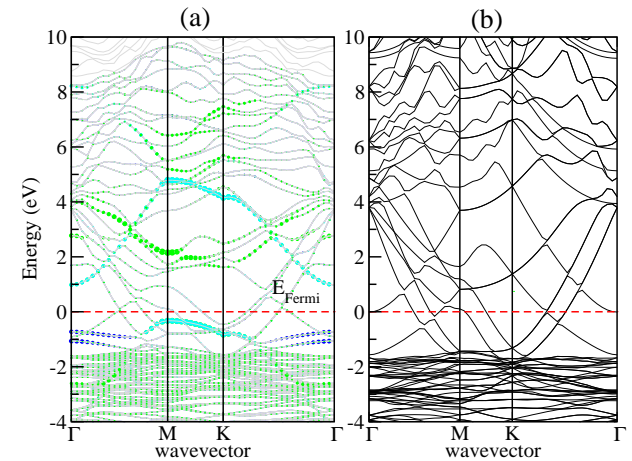


FIG. 1: (color online). Band structure results (energies relative to  $E_{Fermi}$ ). (a) PT SAM on 3 layers of Cu(111). The size of the colored circles is proportional to the projected density of states of each band on a given atom of a molecule: sulfur - blue,  $C_s$  carbons - light blue, and  $C_t$  carbons - green. (b) 3 layer slab of Cu(111). From comparison of (a) and (b) four HOMO and three LUMO bands can be identified due to the SAM attachment.

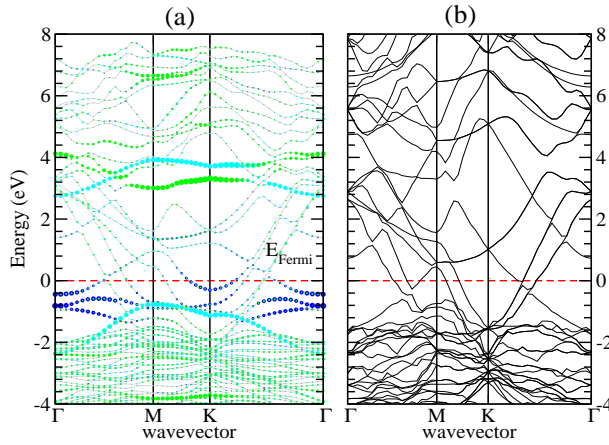


FIG. 2: (color online). Band structure results (energies relative to  $E_{\text{Fermi}}$ ) (a) PT SAM on 3 layers of Au(111). The size of the colored circles is proportional to the projected density of states of each band on a given atom of a molecule: sulfur - blue,  $C_s$  carbons - light blue, and  $C_t$  carbons - green. (b) 3 layer slab of Au(111).

state ( $SS_u$ , at 1.7 eV) are surface states. For the clean Cu(111) these states have energies 0.0 eV and -1.6 eV, respectively, and have similar  $k$  dispersions Fig. (1b). The largest lateral dispersion is due to the bands 1 and 5 originating from the side phenyl carbons ( $C_s$  for short). The minimal separation between such atoms on neighboring PT molecules is 2.61 Å. The molecular bands 2, 6, and 7 are mainly due to the next to sulfur and top carbon atoms ( $C_t$  for short). These  $C_t$  atoms form the longest intermolecular contacts and the lateral dispersion of the  $C_t$ -type bands is not significant compared to that of side carbon  $C_s$ -type bands. There are certainly more electronic states in the band structure due to the SAM, as is evident from the band count in Fig. (1), but these are high energy states (relative to Fermi level) and are not important for the conduction properties of the monolayer. These states are also well delocalized in space such that projected density of states inside the mutual spheres does not give a unique identification of the molecular bands. As will be clear in Section IV, the bands six at 2.8 eV (for point) and the one at 6 eV have the largest contribution to the 2PPE intensity and thus are candidates for the peaks observed by the Zhu et. al. [1].

When the PT is attached to the gold substrate, the bandwidths of all molecular levels are narrower, because the nearest neighbor distance between the molecules is larger due to the larger lattice constant of the underlying substrate. The  $C_s$  atoms on neighboring molecules of the SAM (18° tilted on Au) are separated by at least 3.13 Å from each other, whereas  $C_t$  carbons are 5.0 Å apart (i.e.,  $3R_{\text{Au(Au)}}$ ). The electronic band structures of the SAM /Au(111) and the clean Au(111) surfaces are shown in Fig. (2). The band assignments are summarized in table (I). As in the case of the SAM on Cu, the two

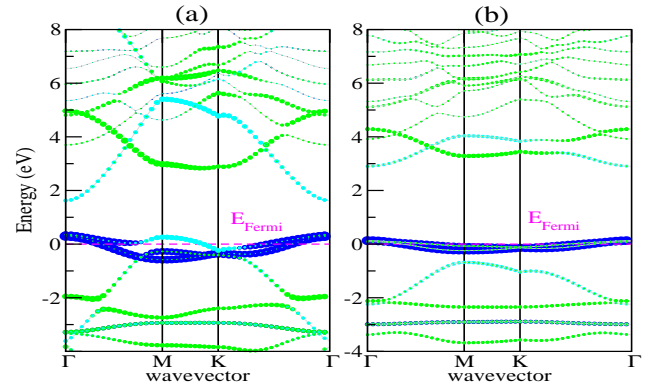


FIG. 3: (color online). (a) Band structure of the free standing array of PT based on the Cu(111) lattice constant and (b) a tilted by 18° PT array based on the Au(111) lattice constant (energies relative to  $E_{\text{Fermi}}$ ). The size of the colored circles is proportional to the projected density of states of each band on a given atom of a molecule: sulfur - blue,  $C_s$  carbons - light blue, and  $C_t$  carbons - green.

nearly degenerate sulfur-based HOMO's (bands 3 and 4) are the molecular levels closest to the Fermi level. As the lattice constant increases (in proceeding from Cu to Au), the direct exchange mechanism responsible for the negative effective mass decays faster than the substrate mediated mechanism. This causes the sign of the effective mass of one of the sulfur bands to become positive on the Au substrate. The most dispersive  $C_s$  bands 1 and 5 have bandwidths smaller by a factor of 2.5 than for the Cu substrate. The occupied surface state  $SS_o$  is strongly hybridized with the sulfur 3p orbitals.

The molecular orbitals closest to the Fermi level  $E_F$  are essential for the conductance properties of the monolayer. In order to enhance conductance it is desirable to reduce the charge injection energy, the energy difference between the Fermi level and the molecular orbital energies of the SAM. We find lateral dispersion significant enough to modify conductance properties of the monolayer in this sense, compared to the single molecule limit. When the HOMO effective mass is positive, the injection energy is smaller and the hole conductance of SAM is higher. To estimate relative contributions of the two mechanisms for the band dispersion we compare the lateral dispersions obtained for the PT arrays in the absence of the substrates (defined as free standing arrays), but maintaining the same geometry as determined with the substrate present. The results of two calculations are shown in Fig. 3. The signs of the 3 and 4 band dispersions are negative and the bandwidth is smaller for the Au(111) case Fig. (3b). In both cases the dispersion of the sulfur bands is larger in the absence of the substrate. This suggests that substrate-mediated interactions has an effect on the bandwidth opposite to that from direct exchange. When the lattice constant is relatively large (i.e. the Au case), the substrate-mediated interaction changes sign in the band 4. The coupling of

the  $C_s$  atoms to the substrate is much smaller, so that substrate-mediated interaction in bands 1 and 5 is much weaker, and the coupling to the substrate is responsible for only 10% of the total bandwidth.

#### IV . 2PPE SPECTRA

The electronic structure of the organic SAM can be directly probed in the photon photoemission experiment [9]. The photon energy is chosen to be less than the work function, such that at least two photons have to be absorbed to remove an electron. There are three electronic states involved in the 2PPE spectra: initial ( $i$ ), intermediate ( $k$ ), and the final ( $f$ ). If one of those states is localized in molecular orbital and the rest of the states are delocalized bulk continuum, then three scenarios are possible for the kinetic energy  $E_{kin}$  behavior with respect to the excitation laser frequency  $\omega_L$ : (1) if  $E_{kin} \sim \omega_L$ , then localized state is initially occupied ( $i$ ); (2) if  $E_{kin} \sim \omega_L$ , then the localized state is intermediate  $k$  below the vacuum level; and (3) if  $E_{kin}$  is independent of  $\omega_L$ , then the localized state is final  $f$  above the vacuum. For the PT-S-C<sub>6</sub>H<sub>6</sub> on Cu(111) two such states are reported: one LUMO above the vacuum at 6.4 eV (relative to  $E_{Fermi}$ ) and another LUMO below the vacuum at 3.3 eV [1].

In the present work we find two states which give rise to the observed 2PPE spectra: LUMO (band 6) at 2.8 eV of the  $C_t$  carbon character and high energy bands at around 6.0 eV whose character is hard to identify at this point due to the hybridization with Cu surface states. This assignment is consistent with the conclusion drawn in [1] based on similarities of spectra taken for the PT and alkanethiolates of different lengths on Cu(111) substrate [1].

There are two possible excitation mechanisms: direct and indirect. In the direct process with one-color pump and probe laser frequencies the 2PPE intensity for  $\perp$ -light polarization is [10, 11]:

$$I^{dir}(i; f; \omega_L) = \frac{(2\pi\omega_L)^2}{E_k - E_i - \omega_L + i\kappa} \sum_{k \ll f} \frac{f_k \langle f | p | k \rangle \langle k | p | i \rangle}{f_i (1 - f_k)} \quad (1)$$

where  $\kappa$  is the lifetime broadening of intermediate level  $k$ . The sum over intermediate states in Eq. (1) includes the interference effects. The delta function is replaced by the Lorentzian to mimic the lifetime of the final state and the laser frequency uncertainty of the pulsed lasers. The result for  $\perp$ -point is shown on Fig. 4 where intensity contributions Eq. (1) are summed over all the initial states  $i$ . The calculated curves were convoluted with Lorentzian function ( $\kappa = 0.1$  eV) to account for the spectrometer resolution. We use intermediate and final level lifetimes  $\kappa = f_k = 0.1$  eV. There is one pronounced peak at about 6.0 eV, whose intensity is resonant with the laser frequency at about 3.6 eV. As the frequency increases the

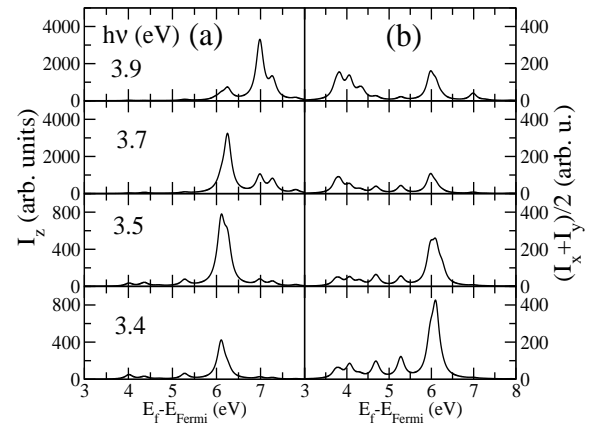


FIG. 4: Prediction of the 2PPE spectra for the direct mechanism according to Eq. (1) for (a) out of plane and (b) in plane light polarizations.

2PPE intensity transfers to higher energies final states ( $> 7$  eV) with 6 eV peak intensity being reduced. The resonance enhancement factor is sensitive to the choice of the damping parameters and even for the large value 0.1 eV used in Fig. (4) the intensity of the out-of-plane polarization varies by the order of magnitude. The resonance effect is related to the large dipole matrix element between the occupied surface state SS<sub>0</sub> and the second LUMO (band 6) separated by 3.7 eV.

For the in-plane polarization there is no strong frequency dependence of 2PPE intensity, because there is no particular pair of states which dominate the sum in Eq. (1). The dipole matrix elements are smaller compared to the out-of-plane polarization and the 2PPE intensity is not resonant with  $\omega_L$ . Therefore the ratio of the out-of-plane and the in-plane polarizations in the direct mechanism model should be resonant with the laser frequency.

In the indirect mechanism the intermediate level can be populated by some incoherent process, for example, by the tunnelling of the photoexcited electron in the substrate to the molecule. In the second step photon removes the photoexcited electron to the vacuum with probability given by the one photon absorption cross-section:

$$I^{indir}(k; f; \omega_L) = \frac{(\omega_L - E_f + E_k) \langle f | p | k \rangle^2}{(1 - f_k) (1 - f_f) f_k (E_{Fermi} + \omega_L)} \quad (2)$$

where  $(1 - f_k)$  and  $f_k (E_{Fermi} + \omega_L)$  factors requires that the intermediate state is empty in equilibrium and can be photoexcited by one photon quanta  $\omega_L$ . It is assumed that all the intermediate states  $k$  have the equal lifetimes and probabilities to be excited in the first step. The result for the two polarizations and the same damping parameters as in direct process is shown in Fig. 5. There are no pronounced resonances and the ratio of the out-of-plane and the in-plane polarizations is relatively independent of the laser frequency. Namely, the ratios of the integrated peak intensities at 6 eV for  $\omega_L = 3.4, 3.5,$

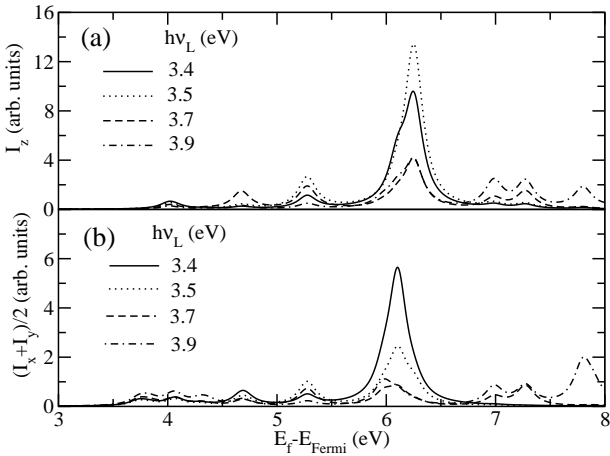


FIG. 5: Substrate assisted 2PPE spectra calculated with Eq. (2) for (a) out of plane and (b) in plane light polarizations.

3.7, and 3.9 are 1.8, 4.6, 3.8, and 4.0 respectively. This is in agreement with the experimentally reported value of  $I_p = I_s = 4$  at  $h\nu_L = 3.7$  eV [1]. Comparison of our analysis with the available experimental data [1] allows us to conclude that the most likely mechanism for the two photon photoemission intensity is indirect. The effect of 2PPE intensity enhancement with the laser frequency was observed for  $\text{SCH}_3$  on  $\text{Ag}(111)$  system by Harris group [12]. This is may be the effect we predict here for the direct mechanism.

## V. WORK FUNCTION CALCULATION

The change of the work function due to the SAM may be employed in the device applications to assist the charge injection into the molecular device [13]. It's important to understand the mechanism of the work function change due to the adsorbates. The work function of a crystal surface is the minimum energy required to remove an electron from the interior of the crystal to a point just outside the crystal [14]. There are two contributions to the work function [15] (1) the electrostatic barrier due to distortion in the charge distribution in surface cells (2) the many-body effects of the screened hole contained in the exchange and correlation contributions to the bulk chemical potential. In some models the distortion in the charge of surface cells is represented as a uniform macroscopic surface density of dipoles and the surface layer is referred to as the 'double layer'. We find electrostatic contribution of polar molecules to be the dominant effect on the work function change.

The unit cell with three metal layers one-side covered by SAM has two inequivalent surfaces. The net dipole moment creates electrostatic potential drop across the vacuum region. For the work function calculations we use six Cu layers substrate covered with SAM from both sides. The inversion symmetry of the supercell with two

equivalent surfaces forces the net dipole to be zero. To separate the electrostatic and exchange correlation contributions to the work function we calculate the averaged surface dipole moment by integrating the charge density of the half of the unit cell:

$$P = \frac{1}{2} \int_{-Z/2}^{Z/2} z [ \langle x; y; z \rangle_{+} - \langle x; y; z \rangle_{-} ] dx dy dz; \quad (3)$$

where planes  $z = 0$  and  $z = Z/2$  contain the inversion centers of the supercell. The Coulomb potential averaged in the lateral direction is shown on Fig. 6 along with the clean substrate and the two SAM arrays in the absence of the substrate for the same geometry. The work function of the clean  $\text{Cu}(111)$  is found to be 5.0 eV in a good agreement with the experimental value of 4.9 eV. The work function of the covered substrate is reduced to 2.7 eV compared with the experimental value of 3.7 eV [1].

To separate the contributions to the work function reduction we first test the double layer model prediction for the SAM layer standing in a free space. Fig. (6b) shows potential drop  $V = 6.5 - 3.8 = 2.7$  eV across the SAM layer with surface dipole  $P_{\text{SAM}} = 1.19$  Debye/molecule, such that potential drop  $4 P_{\text{SAM}} = 2.67$  eV is in good agreement with actual result. The electrostatic contribution to the clean Cu surface work function Fig. (6a) is  $4 P_{\text{Cu}} = 4.6$  eV and exchange-correlation effects contribute another 0.4 eV. In the case of SAM on Cu the net dipole of the double layer approximately equal to sum dipoles in double layers of clean Cu surface and free standing array  $2.06 + 1.19 = 3.25$  Debye. The difference between the simple estimate and the actual result

0.076 Debye is due to the charge transfer at the interface. The laterally average charges densities are shown on Fig. (7, a) for three cases: (1) clean  $\text{Cu}(111)$ ; (2) free standing SAM array without metal substrate; and (3) two-sided SAM /Cu(111). The charge transfer density shown on Fig. (7, b) is very small less than 0.1 e per molecule. Such that the electrostatic contribution to the work function shift can be estimated from the dipole moment of the free standing array of molecules. We calculate the workfunction of the covered substrate to be 2.7 eV with 1.8 eV electrostatic and 0.9 eV exchange-correlation contributions.

The net double layer dipole moment is the key parameter which controls the work function change of the adsorbate surface. To understand the origin of the dipole moment of the free standing array of  $\text{SC}_6\text{H}_6$  molecules we use molecular NLRMOL code [16] to find a dipole moment per molecule 3.33 Debye. This value is significantly larger than the dipole per molecule in the array 1.19 Debye. The nature of the small dipole moment in an array compared to the single molecule result can be resolved by constrained calculations by forcing occupations of two nearly degenerate HOMO orbitals  $p_x$  (in molecular plane orbital) or  $p_z$ . The unconstrained spin non polarized calculations results in 1.88 electrons in  $p_x$  and 1.12 electrons in  $p_z$  orbitals with a net dipole moment of 3.33 Debye. By forcing  $p_z$  orbital being fully occupied the net

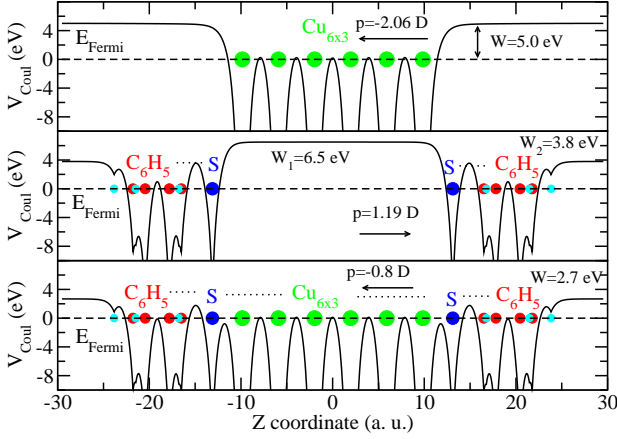


FIG. 6: (color online). Work function and surface dipole calculations for (a) the clean Cu(111), (b) the single monolayer, and (c) SAM on Cu(111).

dipole moment drops to 1.24 D by, which is very close to the SAM value. This suggests that occupation change of the two HOMO orbitals due to the band formation is the primary effect on the net dipole moment.

To reconcile the theory prediction for the work function 2.7 eV and the experimental result 3.7 eV one may assume a lower coverage of the SAM in the experimental system. The larger effective area per molecule is  $A^2 = 21:1$ , where  $A$  is the lateral area and additional factor  $A = 21:1$  is due to the cosine of the tilt angle, which reduces the dipole moment in normal direction. According to our calculations one has to assume  $A = 23.8 \text{ \AA}^2$  to agree with experiment. This estimate is much larger than the  $3 \times 3 \text{ R} 30^\circ$  structure, which suggests  $A = 16:9 \text{ \AA}^2$ . Alternatively, a non-zero kinetic energy of the emitted electrons may account for the discrepancy. Indeed, the Cu/SAM interface consists of two double layers with dipole moments in opposite directions. One layer effectively raises the workfunction whereas the second layer lowers workfunction. This creates a potential barrier for electrons to leave the Cu/SAM surface similar to the Schottky barrier formed at the metal-semiconducting interfaces. Therefore the onset of the one-photon photoemission signal for electrons with zero kinetic energy is suppressed and the measured on-set signal corresponds to the non zero kinetic energy electron emission.

## V I. SUMMARY

We have calculated electronic structure of the SAM phenylthiolate ( $S\text{-C}_6\text{H}_5$ ) on Cu(111) and Au(111) substrates. We found the sulfur HOMO (band 4) to be the closest to the Fermi level for both substrates. We identified four HOMO's and three LUMO's for the both systems. The most dispersive molecular bands are of the side carbon character  $C_s$ . The lateral dispersion of the molecular states modulates the effective charge injection

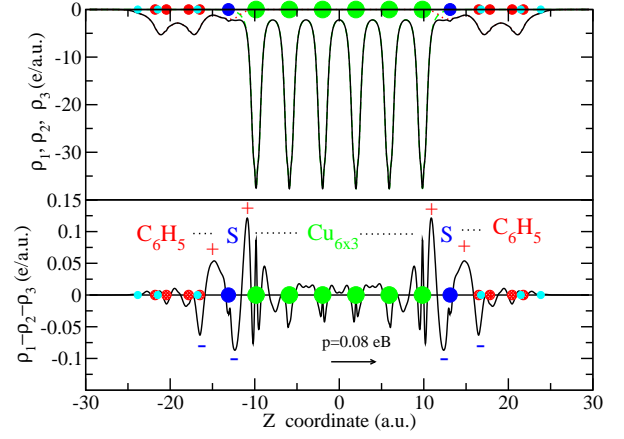


FIG. 7: (color online). (a) Charge density versus z-direction of the Cu(111) (blue), free SAM (red) and attached SAM/Cu(111) (black). (b) Results for the charge density difference and the induced dipole at the contact due to the charge transfer  $p = 0.08$  (D).

energy which leads to the significant differences of the conductance of the monolayer compared to the single molecule. For the closest to the Fermi level sulfur bands we found two competing contributions to the lateral dispersion: (1) the direct wavefunction overlap gives a negative effective mass, whereas (2) the substrate mediated interaction gives a positive effective mass. The overall sign of the effective mass is changed from a negative to a positive value by going from Cu to Au substrate. The latter has a larger lattice constant and the sign change of the effective mass is attributed to the different distance dependencies of the two interactions.

We calculate the 2PPE spectra of the SAM on Cu(111) using the DFT dipole matrix elements for the two mechanisms direct and indirect. In the direct mechanism we predict a very strong intensity dependence of the 2PPE peak. The intensity resonance for the out-of-plane polarization in the direct mechanism happens when the photon energy close to the energy difference between the occupied surface state  $SS_0$  and the molecular state 6. In particular, we predict the order of magnitude intensity enhancement. For the in-plane polarization contributions from several pairs of states in the first step are comparable and only small intensity variation with laser frequency is found. For the indirect mechanism we find a moderate intensity dependence on the excitation photon energy for both polarizations with a nearly constant ratio of the out-of-plane to in-plane signals of about 3-4 in agreement with the experiment [1]. This fact and the absence of the resonant behavior of the 2PPE intensity makes us to conclude that the indirect mechanism contributes the most intensity to the 2PPE peak intensity of resonance A in [1]. The energy positions of the observed molecular states at 6.4 eV and 3.4 eV agree reasonably with our calculations 6.0 eV and 2.8 eV respectively. Those molecular states are mainly due to the next to sulfur carbon

character.

The calculations of the work function due to the SAM coverage of Cu (111) predicts an underestimated value of 2.7 eV compared to the experiment 3.7 eV. We find electrostatic contribution to the work function change 1.8 eV to be mainly due to the dipole moment of the molecules in the absence of the metal substrate. The charge transfer at the metal-molecule interface changes the electrostatic contribution of the work function by only 10%.

Our results suggest the charge injection energy is largely modified due to the lateral dispersion of the molecular bands. Since the conductance properties depends exponentially on the charge injection energy the conductance of the monolayer can not be related to the single molecule conductance. We identify the relative

contributions of the two mechanisms for the lateral dispersion of the sulfur HOMO. Our results can be used to rationalize the conductance properties of the monolayers by changing the underlying substrates or the coverage of the SAM.

#### Acknowledgments

The computations were performed on the BNL galaxy cluster. We are grateful to Mike Weinert, Ben Ocko, and X.-Y. Zhu for helpful discussions. This work was supported in part by DOE Grant No. DE-AC-02-98CH10886.

[\*] Current address: IBM Research Division, T. J. Watson Research Center, Yorktown Heights, New York 10598

- [1] T. Vondrak, H. Wang, P. Winger, C. J. Cramer, and X.-Y. Zhu, *J. Am. Chem. Soc.* **122**, 4700 (2000).
- [2] D. J. Singh, Planewaves, Pseudopotentials and the LAPW Method (Kluwer Academic, Boston, 1994).
- [3] D. J. Singh, *Phys. Rev. B* **43**, 6388 (1991).
- [4] P. Baha, K. Schwarz, and J. Luitz, in *Proceedings of WEN 97* (Techn. Universität Wien, Austria, 1999).
- [5] J. P. Perdew and Y. Wang, *Phys. Rev. B* **45**, 13244 (1992).
- [6] See review by F. Schreiber, *Prog. in Surf. Sci.* **65**, 151 (2000).
- [7] T. Y. B. Leung, P. V. Schwartz, G. Scoles, F. Schreiber, A. Uman, *Surf. Sci.* **458**, 34 (2000).
- [8] M. C. Vargas, P. Giannozzi, A. Selloni, and G. Scoles, *J. Phys. Chem. B* **105**, 9509 (2001).
- [9] X.-Y. Zhu, *Annu. Rev. Phys. Chem.* **53**, 221 (2002).
- [10] O. Madelung, in *Introduction to Solid-State Theory*, edited by M. Cardona, P. Fulde, and H.-J. Queisser (Springer Series in Solid-State Sciences 2, Springer,

Berlin 1981) p. 276.

- [11] M. Wölff, A. Hötzel, E. Knoesel, and D. Velić, *Phys. Rev. B* **59**, 5926 (1999).
- [12] A. D. Miller, K. J. Gane, S. H. Liu, P. Szymanski, S. Garrett-Roe, C. M. Wong, and C. B. Harris, *J. Phys. Chem. A* **106**, 7636, (2002).
- [13] X. Cui, M. Freitag, R. Martel, L. Brus, and P. Avouris, *Nano Lett.* **3**, 783 (2003).
- [14] N. W. Ashcroft and N. D. Mermin, in *Solid State Physics* (Saunders, Philadelphia, 1976) p. 354.
- [15] N. D. Lang, in *Solid State Physics*, edited by Seitz, Turnbull, and Ehrenreich 28 Academic Press, New York 1973 p. 225.
- [16] M. R. Pederson and K. A. Jackson, *Phys. Rev. B* **41**, 7453 (1990); K. A. Jackson and M. R. Pederson, *Phys. Rev. B* **42**, 3276 (1990); M. R. Pederson and K. A. Jackson, *Phys. Rev. B* **43**, 7312 (1991); D. V. Porezag and M. R. Pederson, *Phys. Rev. B* **54**, 7830 (1996); A. Brey, M. R. Pederson, K. A. Jackson, D. C. Patton, and D. V. Porezag, *Phys. Rev. B* **58**, 1786 (1998).